

Geophysical Research Letters

RESEARCH LETTER

10.1029/2019GL082163

Key Points:

- The contribution of transient Antarctic ice sheet variations to Miocene $\delta^{18}\text{O}$ signals is smaller than indicated by equilibrium differences
- Transient ice volume variability is centered around a preferred small state and is dependent on the timescale of the forcing
- Enlarging the West Antarctic land surface increases the self-sustenance of the Miocene Antarctic ice sheet, decreasing the variability

Supporting Information:

- Supporting Information S1

Correspondence to:

L. B. Stap,
lennert.stap@awi.de

Citation:

Stap, L. B., Sutter, J., Knorr, G., Stürz, M., & Lohmann, G. (2019). Transient variability of the Miocene Antarctic ice sheet smaller than equilibrium differences. *Geophysical Research Letters*, 46. <https://doi.org/10.1029/2019GL082163>

Received 22 JAN 2019

Accepted 30 MAR 2019

Accepted article online 4 APR 2019

Transient Variability of the Miocene Antarctic Ice Sheet Smaller Than Equilibrium Differences

L. B. Stap¹ , J. Sutter^{1,2} , G. Knorr¹ , M. Stürz¹, and G. Lohmann¹ 

¹Alfred-Wegener-Institut, Helmholtz-Zentrum für Polar- und Meeresforschung, Bremerhaven, Germany, ²Climate and Environmental Physics, Physics Institute, and Oeschger Centre for Climate Change Research, University of Bern, Bern, Switzerland

Abstract During the early to mid-Miocene, benthic $\delta^{18}\text{O}$ records indicate large ice volume fluctuations of the Antarctic ice sheet (AIS) on multiple timescales. Hitherto, research has mainly focused on how CO_2 and insolation changes control an equilibrated AIS. However, transient AIS dynamics remain largely unexplored. Here, we study Miocene AIS variability, using an ice sheet-shelf model forced by climate model output with various CO_2 levels and orbital conditions. Besides equilibrium simulations, we conduct transient experiments, gradually changing the forcing climate state over time. We show that transient AIS variability is substantially smaller than equilibrium differences. This reduces the contribution of the AIS to $\delta^{18}\text{O}$ fluctuations by more than two thirds on a 40-kyr timescale, hence requiring a larger contribution by deep-sea-temperature variability. The growth rates are much slower than the decay rates, which ensures variability around a preferred small state. Finally, if the bedrock topography enlarges the West Antarctic land surface, AIS self-sustenance increases.

1. Introduction

During the early to mid-Miocene (23 to 14 Myr ago), benthic $\delta^{18}\text{O}$ records show lower values than during the Pleistocene, indicative of a warmer climate and smaller ice sheets (e.g., Cramer et al., 2009; Holbourn et al., 2013; Zachos et al., 2008). In particular, there was probably only limited ice cover on the Northern Hemisphere (Maslin et al., 1998). Moreover, benthic $\delta^{18}\text{O}$ records are fluctuating strongly during this time, most prominently on orbital timescales (Holbourn et al., 2013; Levy et al., 2019; Liebrand et al., 2011; Zachos et al., 2001). This prompts the possibility of large variability of the Antarctic ice sheet (AIS), which at times diminished to sizes considerably smaller than present-day. After the mid-Miocene Climatic Optimum (17 to 14.5 Myr ago), the AIS stabilizes around its present-day size, showing more modest variations (e.g., de Boer et al., 2015; Masson-Delmotte et al., 2010). Benthic $\delta^{18}\text{O}$ records are, however, not only influenced by the AIS volume but also by deep-sea temperatures, and the precise partitioning of the Miocene $\delta^{18}\text{O}$ variations remains under debate (e.g., Bijl et al., 2018; Billups & Schrag, 2002; Holbourn et al., 2013; Langebroek et al., 2010; Lear et al., 2010; Liebrand et al., 2011, 2017; Shevenell et al., 2008). Ice sheet models, particularly of the AIS, driven by Miocene climate forcing, can be used to elucidate this problem from an ice-physical point of view (Barker et al., 1999). To achieve continental-scale variability of the AIS, these models require large local temperature fluctuations of about 10 K, the absolute temperatures being dependent on the mass balance formulation (de Boer et al., 2010; Huybrechts, 1993; Stap et al., 2016). This temperature range has proven to be hard to simulate by climate models, because the associated CO_2 range is very large due to hysteresis in the relation between temperature and CO_2 (Pollard & DeConto, 2005). This hysteresis, which is mainly caused by the ice albedo and the surface-height-temperature feedbacks, results in substantially different CO_2 thresholds for waxing and waning of the AIS. Furthermore, orbital variations can mediate the hysteresis width and therefore affect AIS variability (e.g., Dolan et al., 2011; Langebroek et al., 2009; Pollard & DeConto, 2005; Stap et al., 2017). A recent attempt to model Miocene AIS variability used an isotope-enabled setup of a 3-D ice sheet model coupled to a regional climate model nested in a general circulation model (GCM; Gasson et al., 2016). They performed a set of steady state experiments with CO_2 levels ranging from 280 to 840 ppm and obtained significant variability of the AIS. However, the transiently evolving AIS is not necessarily in equilibrium with the climate. This is because the change in AIS volume over a given period of time is limited by the rates of accumulation and ablation. Furthermore, the hysteresis in the CO_2 -temperature relation may result in different simulated ice volumes for warming and cooling

climates at the same CO₂ level. Hence, transient variability of the AIS remains uncertain. Here, we take a first step to resolve this issue. We study the impact of CO₂ changes on AIS variability during the Miocene, using an ice sheet model forced by output of a coupled atmosphere-ocean GCM (Stärz et al., 2017). Steady state simulations are started from conditions without ice and with a present-day AIS. Moreover, we perform transient runs by using an index method to interpolate between different forcing climate states. Lastly, we investigate the influence of several other factors, namely, orbital variability, and bedrock topography, on our simulated Miocene AIS variability, as well as the sensitivity to the model parameter related to the lapse rate correction precipitation.

2. Models and Methods

In this study, we carry out simulations of the AIS using the 3-D thermodynamical Parallel Ice Sheet Model (PISM) version 0.7.3 (Bueler & Brown, 2009; Winkelmann et al., 2011). A comprehensive description of the configuration of PISM can be found in section S1 in the supporting information (Aschwanden et al., 2012; Bauer & Ganopolski, 2017; Beckmann & Goosse, 2003; Bueler & Brown, 2009; Bueler et al., 2007; Depoorter et al., 2013; Fretwell et al., 2013; Greve, 2001; Lingle & Clark, 1985; Rignot et al., 2013; Ritz et al., 2001; Schodlok et al., 2016; Shapiro & Ritzwoller, 2004; Stocchi et al., 2013; Uppala et al., 2005; van de Berg et al., 2011). In brief, we use a 16 × 16-km resolution grid covering the whole Antarctic continent. PISM calculates grounded ice velocities using a superposition of the commonly used shallow ice approximation and shallow shelf approximation. This method ensures a smooth transition of the velocities toward the floating ice shelf, where only the shallow shelf approximation is used. Calving is simulated in two ways: (1) using a kinematic first-order calving law, named *eigen-calving* (Levermann et al., 2012), and (2) floating ice reaching grid points where the ocean depth exceeds 2000 m is removed, as are icebergs. Surface melt follows from a positive degree day scheme (Braithwaite, 1984; Hock, 2005; Reeh, 1991), while subshelf melt is calculated using a quadratic temperature relation (based on Beckmann & Goosse, 2003).

Atmospheric and oceanic input data are obtained from simulations using the coupled atmosphere-ocean GCM COSMOS (Jungclaus et al., 2006), which are described in detail in Stärz et al. (2017). COSMOS is run into equilibrium using dynamical vegetation (Brovkin et al., 2009; Raddatz et al., 2007), and a global topography representing the mid-Miocene (Herold et al., 2008; Figure S1 for the Antarctic surface elevation). Orbital conditions are kept constant at present-day settings. We use output of three simulations, with different CO₂ levels (278, 450, and 600 ppm) covering the wide range suggested by different proxy records (Badger et al., 2013; Foster et al., 2012; Greenop et al., 2014; Kürschner et al., 2008; Zhang et al., 2013). From the final-100-year average of these simulations, we determine monthly precipitation, surface temperature, and yearly 3-D ocean temperature anomalies with respect to an equilibrium preindustrial (PI) run. The surface temperature and precipitation anomalies are remapped to the PISM grid using a flux-conserving method and added to a base climate provided by the 1970–2000 average of ERA-40 reanalysis data (Uppala et al., 2005; Figures S2 and S3). During the course of all runs, surface temperatures are corrected for surface height changes with respect to the PI reference, induced by altering ice thickness and bedrock elevation. For this purpose, we use a constant temperature lapse rate of 8.0 K/km, while we refrain from using a precipitation lapse rate. The impact of (the lack of) these lapse rates is investigated below. The ocean temperature anomalies are added to the 1955–2006 average of the World Ocean Database 2009 data set (Locarnini et al., 2010; Figure S4 for the surface temperature). We use an anomaly approach rather than absolute values from the climate model output. This is because simulating the present-day Antarctic climate remains a challenge for all climate models, and the anomaly approach reduces systematic errors yielded by climate models (Huybrechts et al., 2004). Moreover, the native resolutions of these base climates are higher than that of COSMOS, and hence, the reference climate is more detailed. A bias is induced, however, because we use present-day base climates, which represent a slightly warmer climate state than our PI reference. Below, we show that using the anomaly approach in our model setup is essential for obtaining large differences between the high- and low-CO₂ equilibrium results. All simulations are started with two spinup phases of 100 years and 200 kyr without ice mass changes, to smooth and stabilize the initial conditions.

We perform steady state and transient experiments using PISM. For the steady state simulations, the initial ice sheet and bedrock topographies are taken from the Bedmap2 reconstruction (Fretwell et al., 2013). Alternatively, the ice sheet is first removed and the bedrock has been allowed to rebound. Hence, in the latter runs, the initial surface height is different from the PI reference, and therefore, the forcing at the beginning of the run is already corrected for surface height changes. After the spinup, we use constant forcing with PI

conditions, or Miocene conditions with the three different CO₂ levels (MIO_low, MIO_med, and MIO_high) for 200 kyr. Additionally, we use Miocene conditions in between the low and medium, and medium and high CO₂ levels, by taking the average of the two forcing climates. Only the equilibrated final state is used for analysis.

The transient simulations are initialized from the steady state solutions for ice thickness, ice temperature, and bedrock height of the MIO_low (cold start), or the MIO_high (warm start) simulation. The climate forcing in these runs is interpolated between the forcing fields used in the MIO_low, MIO_med, and MIO_high simulations ($F_{i,j}(\text{MIO_low})$, $F_{i,j}(\text{MIO_med})$, and $F_{i,j}(\text{MIO_high})$). To this end, we use an index method adapted from Sutter et al. (2016). The surface air temperature, precipitation and ocean temperature fields at any given time ($F_{i,j}(t)$) are determined by a CO₂ index $g(t)$ ranging from 0 to 1, using

$$F_{i,j}(t) = F_{i,j}(\text{MIO_low}) \cdot \frac{g_{\text{MIO_med}} - g(t)}{g_{\text{MIO_med}}} + F_{i,j}(\text{MIO_med}) \cdot \frac{g(t)}{g_{\text{MIO_med}}} \quad (1)$$

when $g(t) < g_{\text{MIO_med}}$, and

$$F_{i,j}(t) = F_{i,j}(\text{MIO_high}) \cdot \frac{g(t) - g_{\text{MIO_med}}}{1 - g_{\text{MIO_med}}} + F_{i,j}(\text{MIO_med}) \cdot \frac{1 - g(t)}{1 - g_{\text{MIO_med}}}, \quad (2)$$

when $g(t) > g_{\text{MIO_med}}$, and where $g_{\text{MIO_med}} = \frac{450-278}{600-278} = 0.5342$.

In this study, we aim to demonstrate the difference between equilibrated and transient AIS variability. For this purpose, our model setup has two benefits: (1) it is computationally less expensive than more sophisticated coupled ice sheet-climate models, enabling us to perform transient simulations on long ($10^5 - 10^6$ years) timescales, as well as a suite of sensitivity experiments, and (2) as a first step it shows the mono-causal effect of the ice sheet dynamics, not obscured by the more unconstrained ice sheet-climate feedbacks. To exactly locate the CO₂ threshold for (de)glaciation, however, more complex coupled ice sheet-climate model approaches (e.g., Gasson et al., 2016) are better suited. We therefore refer to CO₂ concentrations in a relative (low, medium, and high) rather than absolute sense. Here, the equilibrated ice sheets rather serve to indicate the potential ice volume variability during the Miocene as a result of CO₂ changes.

3. Results and Discussion

3.1. Equilibrated Miocene AIS Variability

The steady state simulations show a largely varying AIS size between different CO₂ levels (Figure 1 and Table S1). The climate forcing of the MIO_low simulation differs from the reference PI forcing in global paleogeography and albedo due to dynamic vegetation cover changes. During the Miocene, more precipitation falls on the AIS (Figure S2b). This gives rise to an increase in modeled ice sheet height on the eastern part of the continent (Figures 1a and S5b). Concomitantly, air temperatures are higher, leading to substantial surface melt on the warmer western part (Figure S3b). Consequently, we simulate a significantly smaller West AIS (WAIS), with ice domes only left on high land, namely, on the Executive Committee Range, along the Bellinghousen Sea, and on the Peninsula (Figure 1a). In the MIO_med simulation, these domes have melted away, and surface melt has started to affect a large part of the East AIS (EAIS) as well (Figure 1b). Dome C is ice free, along with its drainage sectors (Wilkes Land, Terre Adelie, and George V Land). When the AIS has equilibrated at the high CO₂ level, only the high parts of Dronning Maud Land and the Transantarctic Mountains remain glaciated (Figure 1c). The difference between the low and high CO₂ climate states is substantial (Figure 1d), amounting to 46 m sea level equivalent (m.s.l.e.; Table S1). It is reduced to 39 m.s.l.e. when the runs are started with a deglaciated rebounded topography (Table S1). Removal of the ice sheet lowers the surface considerably. Hence, the forcing surface temperatures are increased, as they are lapse rate corrected to a lower elevation. This causes the simulated low-CO₂ ice sheet to be smaller in this case (Figures S6a and S6b). There is particularly strong hysteresis at the medium-CO₂ climate, as considerably less ice volume is obtained when the run is started with a deglaciated rebounded bedrock (Figures S6c and S6d).

The large variability in these simulations suggests that the threshold for glaciation and deglaciation is crossed at a CO₂ level of ~450 ppm. The modeled behavior of the AIS is, however, dependent on the specific combination of climate and ice sheet model we employ (de Boer et al., 2015; Dolan et al., 2018; Gasson et al., 2014). Furthermore, the threshold is affected by our experimental design. As is shown in Stärz et al. (2017), the climate state of COSMOS is relatively sensitive to changes in CO₂ and boundary conditions. Changes in

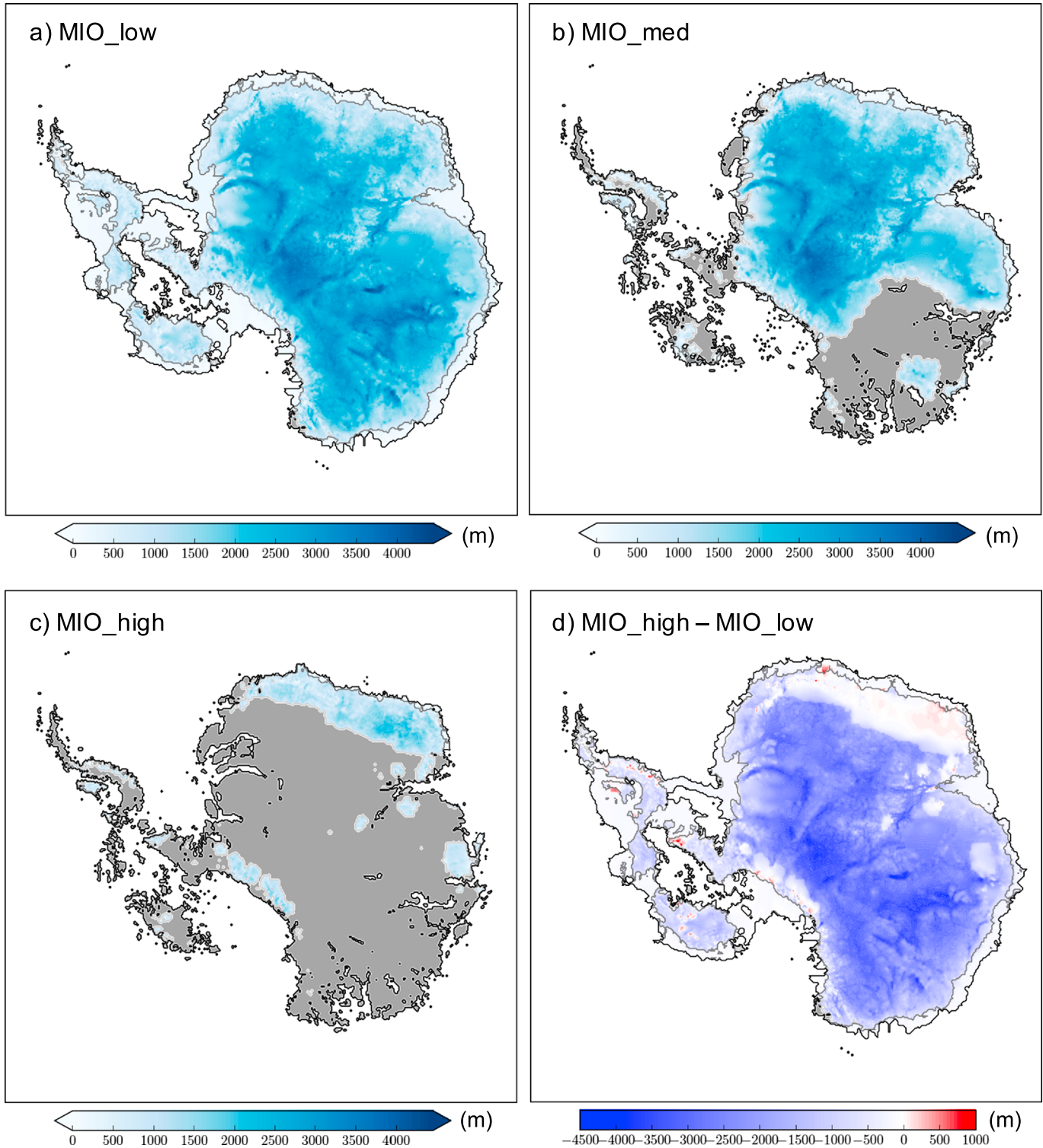


Figure 1. Equilibrated ice thickness from the steady state simulations, using a present-day topography (Bedmap2), and a base climate provided by ERA-40 reanalysis data in the ice sheet model: (a) MIO_low, (b) MIO_med, and (c) MIO_high. (d) Ice thickness difference between MIO_high and MIO_low, indicating the potential variability during the Miocene. The gray line indicates the edge of the grounded ice sheet; the black line shows the edge of the continent or ice shelf. In (d) the edges for the simulation MIO_low are shown. Gray areas indicate land that is not glaciated.

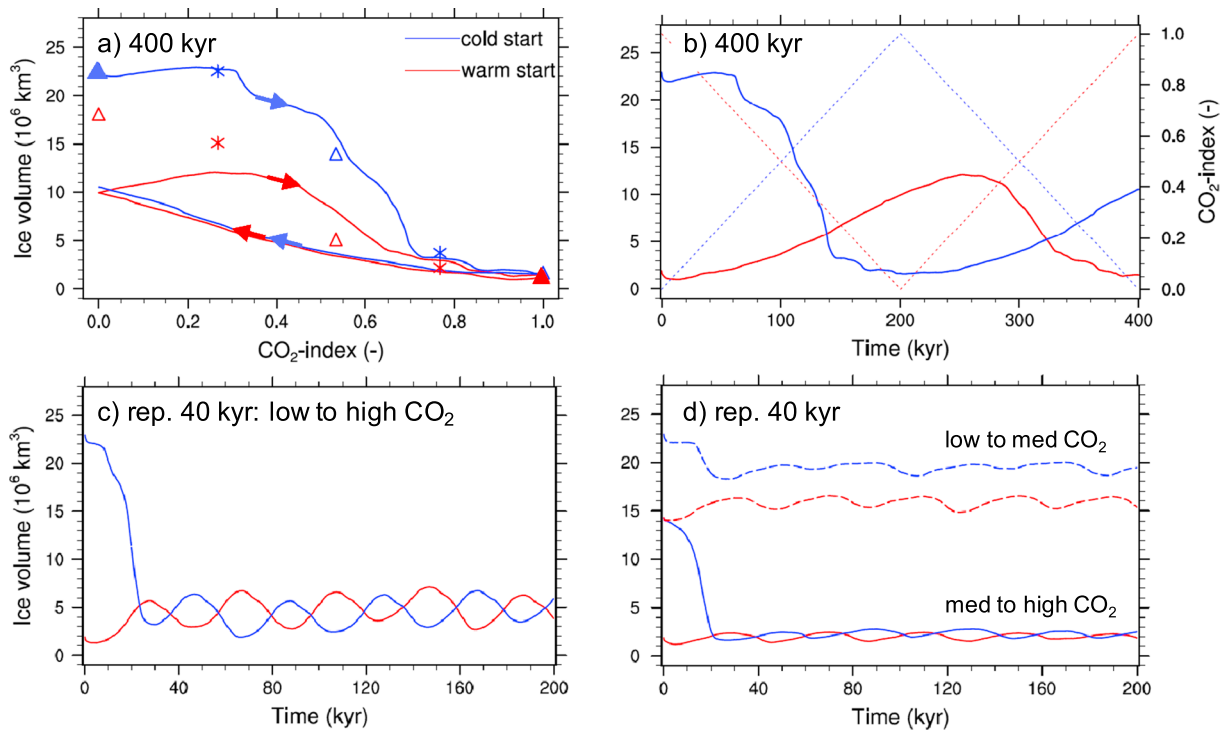


Figure 2. (a) Ice volume against CO_2 in the transient index run in which CO_2 is cycled over 400 kyr between low and high levels. The runs are started from cold conditions (blue) or warm conditions (red; filled triangles). The direction of ice volume progression is indicated by arrows. Triangles indicate the results of the steady state runs using Miocene climates; asterisks indicate the results of the runs using interpolated climates. (b) Ice volume (thick solid line) and the CO_2 index (thin dotted line) over time in the same run. (c) Ice volume over time in the transient index runs in which CO_2 is cycled five times over 40 kyr between low and high levels. (d) Same as (c), for index cycles between low and medium CO_2 (dashed lines), and between medium and high CO_2 (solid lines).

topographic boundary conditions from PI to the Miocene conditions lead to a global warming of 2.4 K, while keeping atmospheric CO_2 at PI levels. Using a similar setup, Goldner et al. (2014) found the same increase from a PI configuration to Miocene conditions at 400 ppm CO_2 , but their climate model CESM1.0 is significantly less sensitive to CO_2 changes. Furthermore, our forcing temperatures are slightly warm biased, due to a PI-PD discrepancy in the base climate (see section 2). The usage of a base climate instead of absolute values from COSMOS is critically important—see Figure S7 for the yearly averaged difference in forcing—as the equilibrated ice volume differences are severely reduced when applying the latter (Figure S8 and Table S1). In the following, we focus on the results of the anomaly approach since they show the difference between equilibrium and transient variability more distinctly. For the above reasons, the CO_2 threshold is relatively low in our simulations. Although this is in broad agreement with proxy- CO_2 data (Badger et al., 2013; Foster et al., 2012; Greenop et al., 2014; Kürschner et al., 2008; Zhang et al., 2013), other studies using more complex ice sheet-climate model setups generally find both the glaciation and deglaciation thresholds at higher CO_2 levels (e.g., Gasson, 2013; Gasson et al., 2014, 2016; Pollard & DeConto, 2005; Pollard et al., 2015). The equilibrated Miocene ice sheets we simulate at different CO_2 levels are also smaller than those simulated by Gasson et al. (2016). In light of these considerations, the relatively low CO_2 range in our simulations should only be regarded as the background for the difference between equilibrium and transient simulations that we explore.

In the next part, we will investigate how much variability we obtain in simulations, in which the forcing climate is gradually varied between high and low CO_2 conditions.

3.2. Transient Miocene AIS Variability

Simulations with the index method are initialized either with high (warm start) or low (cold start) CO_2 climate forcing, starting from the equilibrated state, and cover one complete cycle. First, we conduct a quasi-orbital 400-kyr cycle, giving the ice sheet a long time to adapt to the changing climate forcing. Starting from cold conditions, the ice sheet volume decreases relatively slowly at first when the CO_2 index (g) is lower than 0.5 (Figure 2a, blue line). At medium CO_2 levels, the ice volume is close to equilibrium states

calculated from the steady state experiments (Figure 2a, symbols). Increasing CO_2 crossing $g = 0.5$, stronger surface melt due to warmer surface air temperatures turns the mass balance negative over a large part of the interior ice sheet, and mass loss is accelerated. At around $g = 0.7$, the ice sheet is almost at its equilibrium minimum size.

Growth of the ice sheet is limited by the rate of precipitation, which is generally small over Antarctica. Therefore, lowering CO_2 leads to a slow regrowth in AIS ice volume, which remains smaller than its equilibrium size (Figures 2a and 2b, blue and red lines). The results for the warm start and the cold start simulations are similar for the descending CO_2 branch. At the minimum CO_2 level, the ice sheet is at little over half (55%) the equilibrium volume (Figure S9a). The total transient variability is larger, amounting to approximately two thirds of the equilibrium variability. This is because the ice sheet is still adapting to the colder climate when CO_2 is already increasing again in the warm start simulation (Figure 2b). Therefore, the AIS initially continues to expand, which means that even on these long timescales growing ice volume with increasing CO_2 seems possible. The induced hysteresis from this delayed response is only manifested in transient simulations. It differs from earlier described hysteresis due to the difference in surface height and albedo caused by the absence or presence of an ice sheet (e.g., Abe-Ouchi et al., 2013; Oerlemans, 1980; Pollard & DeConto, 2005), which is also visible in our equilibrated results.

At around $g=0.5$, the surface mass balance becomes significantly negative again. This leads to strong enough ice sheet decay, such that the AIS reaches its equilibrium size again at the maximum CO_2 level. In the time spectrum the delayed peak for the increasing ice sheet is also clearly visible, while the ice sheet volume follows the forcing more closely when it is waning (Figure 2b). We show that the periodicity of the applied CO_2 cycles has a dominant effect on ice sheet hysteresis. For instance, when the full CO_2 cycle is imposed over only 40 kyr, mimicking the obliquity frequency, the growing ice sheet is further from equilibrium than in the 400-kyr run (Figures S10a and S10b). Still, surface melt steers the ice sheet quite quickly toward its small state during warm conditions ($g > \sim 0.5$). However, returning to colder conditions, the AIS has even less time to regrow, which prevents the AIS from recovering to its initial conditions. At the minimum CO_2 level, the ice sheet size now only reaches $5.1 \cdot 10^6 \text{ km}^3$, roughly 28% of the equilibrium volume (Figure S9b). Conversely, if an (ad hoc) 1,600 kyr CO_2 cycle is applied, the ice sheet almost completely recovers, to about 83% of the equilibrium volume at the lowest CO_2 level (Figures S9c, S10c, and S10d). Our results therefore do not contradict earlier studies that varied climate forcing over million year timescales and found equilibrium and transient AIS responses to be comparable (Gasson et al., 2014; Pollard & DeConto, 2005).

3.3. Impact of Short Timescale Variability on the $\delta^{18}\text{O}$ Signal

Next, we investigate the transient behavior of the AIS when it is subject to repeated short timescale climate variability (Figures 2c and 2d). We perform simulations in which the CO_2 index is linearly varied, in the same manner as before, five consecutive times over 40 kyr. The whole simulated period is therefore 200 kyr. When CO_2 is varied between low and high levels, we obtain an ice sheet ranging between 2 and $7 \cdot 10^6 \text{ km}^3$ ice volume. This is between 9% and 30% of the present-day ice sheet volume, and equivalent to a 12.7-m difference in sea level.

From our results, we estimate $\delta^{18}\text{O}_{\text{SW}}$ variability by considering a range of 0.85 to 1.08 $\delta^{18}\text{O}_{\text{SW}}/100 \text{ m.s.l.e.}$ (Langebroek et al., 2010). The 40-kyr variability of $5 \cdot 10^6 \text{ km}^3$ ice volume (Figure 2c) is then equivalent to 0.11‰ to 0.14‰ $\delta^{18}\text{O}_{\text{SW}}$. The cold start and warm start simulations converge quickly toward a relatively small state, due to the earlier described difference between the growth and decay rates. The preferred small state implies generally low $\delta^{18}\text{O}_{\text{SW}}$ values. Such low values, 1.80‰ (PI value= 3.23‰) on average, are shown by the stacked benthic $\delta^{18}\text{O}_{\text{SW}}$ record of Zachos et al. (2008) over the period 16.5 to 15 Myr ago. By taking the root of the squared difference between this record interpolated to 1-kyr resolution and the 400-kyr running average and multiplying by 2, we determine a mean variability of 0.20‰ during this time. Our model therefore explains 55% to 70% of the variability in the data. Because of the difference in timescale for a growing and decaying ice sheet, it is difficult to model variability with a larger ice sheet on average. Meanwhile, the observed benthic $\delta^{18}\text{O}_{\text{SW}}$ (Zachos et al., 2008) shows a similar variability of 0.21‰ with a larger average of 2.24‰, which suggests a large Antarctic ice volume, during the period 19.0 to 17.5 Myr ago. In light of our results, this would require a higher contribution of deep-sea temperature and perhaps the Greenland ice sheet to the $\delta^{18}\text{O}_{\text{SW}}$ variability during this time.

In simulations in which CO_2 ranges between medium and high (Figure 2d, solid lines), and between low and medium levels (Figure 2d, dashed lines), we obtain small variability. In the former case, surface melt

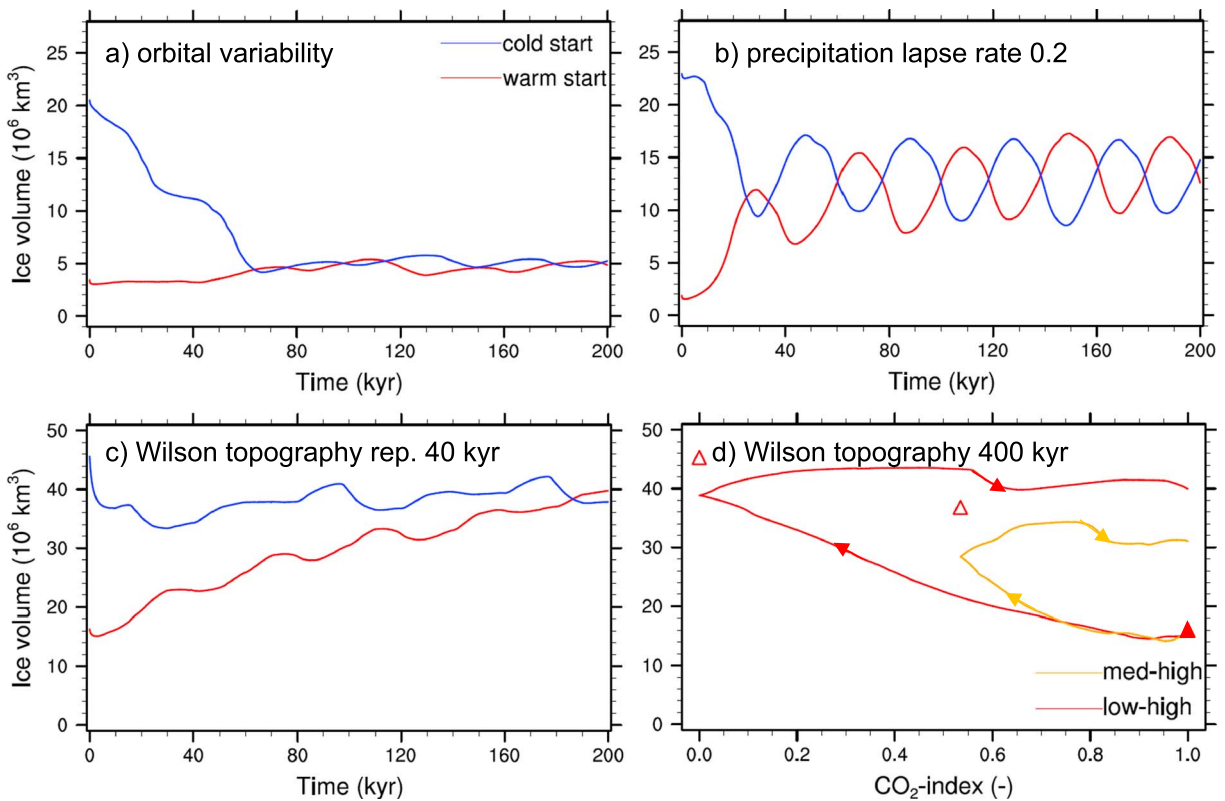


Figure 3. (a–c) Ice volume over time in the transient index runs in which CO_2 is cycled five times over 40 kyr between low and high levels, using (a) orbital (obliquity) variability around the medium- CO_2 climate state, (b) a $0.2 \text{ m}\cdot\text{year}^{-1}\cdot\text{km}^{-1}$ precipitation lapse rate instead of $0.0 \text{ m}\cdot\text{year}^{-1}\cdot\text{km}^{-1}$, and (c) a late Eocene topography (Wilson et al., 2012) in the ice sheet model. The runs are initialized from equilibrated cold conditions (low CO_2 ; blue) or warm conditions (high CO_2 ; red). (d) Ice volume against CO_2 in the transient index run in which CO_2 is cycled over 400 kyr between low and high levels (red), or between medium and high levels (orange), starting from equilibrated warm conditions (high CO_2 ; filled triangle) using the late Eocene topography in the ice sheet model. The direction of ice volume progression is indicated by arrows. Triangles indicate the results of the steady state runs using Miocene climates.

stays sufficiently high so that ice sheet growth is very limited. In the latter case, we simulate a very stable ice sheet with a large volume, which depends on the initial condition. Crossing the (de)glaciation threshold, wherever located, is hence a prerequisite for obtaining significant ice volume variability.

3.4. Other Influencing Factors

In this section, we investigate the influence of several factors other than CO_2 , namely, orbital variability, ocean temperatures, and bedrock topography, on our simulated Miocene AIS variability. Furthermore, we perform sensitivity studies on model parameters related to the lapse rate correction of temperature and precipitation. In section S2 (Fortuin & Oerlemans, 1990), we additionally analyze the influence of ocean temperatures and the lapse rate correction for atmospheric temperature.

First, we repeat our steady state and 40-kyr variability experiments, including orbital variations. The input for these runs is taken from COSMOS output of simulations using 450 ppm (medium) CO_2 in combination with high (24°) and low obliquity (22°), or alternatively with perihelion during Southern Hemisphere summer and winter (Stärz; 2013; see also section S1). The steady state ice volume difference between the AIS during high- and low-obliquity orbits is $9.5 \cdot 10^6 \text{ km}^3$ (22.5 m.s.l.e.) when starting from a deglaciated and rebounded modern bedrock topography (Table S1). The difference between perihelion during Southern Hemisphere summer and winter is similar at $9.9 \cdot 10^6 \text{ km}^3$ (23.6 m.s.l.e.). Just as for the simulations using different CO_2 levels, only a small part of this ice volume variability is shown in the transient experiment (Figure 3a for the obliquity simulations). The results of our orbital simulations imply that transient ice volume variability is smaller than equilibrium differences, irrespective of how the climate forcing signals are constructed. In reality, the temperature and precipitation signals imposed on the ice sheet are induced by a combination of CO_2 and orbital changes. These changes may enhance or diminish each other's impacts, depending on if they are synchronous.

Second, earlier modeling studies have used different ways to correct precipitation for surface height changes (e.g., Charbit et al., 2002; Gasson et al., 2014; Kirchner et al., 2011; Quiquet et al., 2012; Yamagishi et al., 2005; Yan et al., 2016). We refrain from using a precipitation lapse rate correction in our reference experiments. By repeating our 40-kyr variability simulation, we investigate the impact of using a lapse rate of $0.2 \text{ m}\cdot\text{year}^{-1}\cdot\text{km}^{-1}$. This lapse rate is determined by calculating the mean precipitation change per unit temperature change over the Antarctic domain in the forcing COSMOS runs, which yields $0.025 \text{ m}\cdot\text{year}^{-1}\cdot\text{K}^{-1}$, and multiplying with our reference temperature lapse rate of $8.0 \text{ K}/\text{km}$. The minimal volume of the AIS is larger in this case, because of the increased precipitation at high CO_2 levels (Figure 3b). This is mainly a consequence of increased ice sheet height, and also the ice sheet area is more extensive (not shown). We deduce that a good representation of precipitation is of vital importance for the simulation of the Miocene AIS. The transient ice volume variability between high and low CO_2 levels is now slightly larger than before at approximately $6 \cdot 10^6 \text{ km}^3$ (15.2 m.s.l.e.). Nevertheless, it remains significantly smaller than the equilibrium variability. In the colder and drier Pleistocene climate, on the one hand precipitation rates are smaller, which would slow down the growth of the AIS further. On the other hand, equilibrium differences are also smaller, and would therefore be attained more easily in transient simulations.

Lastly, Antarctic bedrock topography is known to have a significant influence on simulated paleo-ice volume (e.g., Austermann et al., 2015; Gasson et al., 2015, 2016; Huybrechts, 1993; Oerlemans, 1984; Siegert, 2008; Wilson et al., 2013). A recent study found that the evolution of the Antarctic continental shelf over the past 34 Myr has severely changed the sensitivity of the AIS to climatic forcings (Colleoni et al., 2018). The Antarctic bedrock topography during the Miocene is, however, very uncertain, and no consensus map has been published as of yet. In our reference simulations, we therefore use a present-day Antarctic topography in the ice sheet model. Since Miocene topography was surely different from present-day (De Santis et al., 1999; Huang et al., 2014), we perform additional 400-kyr and repeated 40-kyr variability experiments, using the Late Eocene topography of Wilson et al. (2012; extensively discussed in section S3; Lythe & Vaughan, 2001; Wilson et al., 2012). In short, the ice sheet shows different behavior in this case (Figures 3c and 3d and Table S1). In general, self-sustenance of the AIS is increased. This is because the ablation area of the EAIS is reduced by the presence of a large WAIS in these runs. Mass loss due to surface melt is therefore reduced on the EAIS, causing it to grow much thicker when CO_2 is decreased. A thicker ice sheet leads to a stronger height correction for temperature, thereby strengthening the surface-height-temperature feedback. Therefore, the EAIS retreats much less when CO_2 is increased again. In these runs, the late Eocene topography used in the ice sheet model differs significantly from the topography that is used in the climate forcing. Hence, the climate forcing is strongly determined by the (lack of) surface height correction for temperature and precipitation. Further research on this issue, preferably using a coupled ice sheet-climate model, is needed to more rigorously assess the influence of bedrock topography on AIS dynamics. Nevertheless, in agreement with Colleoni et al. (2018), we identify bedrock topography as a source of considerable uncertainty in the evolution of the Miocene AIS.

4. Conclusions

The early to mid-Miocene represents an essential period to test ice sheet models, since large benthic $\delta^{18}\text{O}$ fluctuations are recorded during this time, which potentially indicate large continental-scale AIS variability not displayed after this time (Bijl et al., 2018; Billups & Schrag, 2002; Holbourn et al., 2013; Langebroek et al., 2010; Lear et al., 2010; Levy et al., 2019; Liebrand et al., 2011, 2017; Shevenell et al., 2008). Here, we have shown that considering modeled equilibrium states of the Miocene AIS considerably overestimates transient AIS variability.

We have first performed equilibrium simulations under three different CO_2 levels. These show a large ice volume difference of $16.8 \cdot 10^6 \text{ km}^3$ ($39 > \text{m.s.l.e.}$). However, in transient simulations, in which CO_2 is gradually changed between the extreme levels over the course of 400 kyr, only about two thirds of this variability is attained. When the length of the CO_2 cycle is decreased to 40 kyr, the transient variability is even smaller at approximately $5 \cdot 10^6 \text{ km}^3$ (12.7 m.s.l.e.). Smaller variability means a reduced contribution of the AIS to the $\delta^{18}\text{O}$ signal during the Miocene, warranting a larger contribution from deep-sea temperature changes.

The decay rate of the AIS is relatively fast in our simulated CO_2 range, such that high CO_2 levels quickly yield a small AIS. However, the growth rate is significantly smaller due to limited precipitation on the AIS, which impedes equilibration of the AIS at low CO_2 levels. The variability is therefore centered around a preferred

small state. The slower growth than decay rates also cause ice volume hysteresis to gradual forcing, enabling ice growth when CO₂ increases.

The sensitivity studies we performed show that increased levels of precipitation during the Miocene, resulting from the introduction of a precipitation lapse rate, lead to larger equilibrium states at high CO₂ levels. A substantial difference between equilibrium states and transient variability of the AIS is, however, still present. Furthermore, changing bedrock topography has the potential to significantly alter the transient dynamics of the AIS, and therefore, it represents a factor of large uncertainty in the evolution of the Miocene AIS. Experiments forced by climate anomalies resulting from orbital and CO₂ changes show qualitatively similar behavior, meaning transient ice volume variability is smaller than equilibrium differences regardless of how the climate forcing signals are constructed.

Acknowledgments

The data presented in this paper are available at <https://doi.pangaea.de/10.1594/PANGAEA.889802> website. This paper contributes to PACES-II, the Helmholtz Research Programme of the Alfred Wegener Institute. Computer simulations were performed on the Cray CS400 (“Ollie”) supercomputer of AWI. We thank Edward Gasson and anonymous reviewers for their constructive comments, which have helped us to improve the quality of the paper. We further thank Thomas Kleiner for extensive technical support, Christian Rodehacke for discussions on the Antarctic ice sheet, and Bas de Boer for supplying the ERA-40 data for Antarctica.

References

- Abe-Ouchi, A., Saito, F., Kawamura, K., Raymo, M. E., Okuno, J., Takahashi, K., & Blatter, H. (2013). Insolation-driven 100,000-year glacial cycles and hysteresis of ice-sheet volume. *Nature*, *500*(7461), 190.
- Aschwanden, A., Bueler, E., Khroulev, C., & Blatter, H. (2012). An enthalpy formulation for glaciers and ice sheets. *Journal of Glaciology*, *58*(209), 441–457.
- Austermann, J., Pollard, D., Mitrovica, J. X., Moucha, R., Forte, A. M., DeConto, R. M., et al. (2015). The impact of dynamic topography change on Antarctic ice sheet stability during the mid-Pliocene warm period. *Geology*, *43*(10), 927–930.
- Badger, M. P. S., Lear, C. H., Pancost, R. D., Foster, G. L., Bailey, T. R., Leng, M. J., & Abels, H. A. (2013). CO₂ drawdown following the middle Miocene expansion of the Antarctic Ice Sheet. *Paleoceanography*, *28*, 42–53. <https://doi.org/10.1002/palo.20015>
- Barker, P. F., Barrett, P. J., Cooper, A. K., & Huybrechts, P. (1999). Antarctic glacial history from numerical models and continental margin sediments. *Palaeogeography, Palaeoclimatology, Palaeoecology*, *150*(3–4), 247–267.
- Bauer, E., & Ganopolski, A. (2017). Comparison of surface mass balance of ice sheets simulated by positive-degree-day method and energy balance approach. *Climate of the Past*, *13*(7), 819.
- Beckmann, A., & Goosse, H. (2003). A parameterization of ice shelf–ocean interaction for climate models. *Ocean Modelling*, *5*(2), 157–170.
- Bijl, P. K., Houben, A. J. P., Hartman, J. D., Pross, J., Salabarnada, A., Escutia, C., & Sangiorgi, F. (2018). Paleocene and ice sheet variability offshore Wilkes Land, Antarctica—Part 2: Insights from Oligocene-Miocene dinoflagellate cyst assemblages. *Climate of the Past*, *14*(7), 1015–1033.
- Billups, K., & Schrag, D. P. (2002). Paleotemperatures and ice volume of the past 27 Myr revisited with paired Mg/Ca and 18O/16O measurements on benthic foraminifera. *Paleoceanography*, *17*(1), 1003. <https://doi.org/10.1029/2000PA000567>
- Braithwaite, R. J. (1984). Calculation of degree-days for glacier-climate research. *Zeitschrift für Gletscherkunde und Glazialgeologie*, *20*, 1–8.
- Brovkin, V., Raddatz, T., Reick, C. H., Claussen, M., & Gayler, V. (2009). Global biogeophysical interactions between forest and climate. *Geophysical Research Letters*, *36*, L07405. <https://doi.org/10.1029/2009GL037543>
- Bueler, E., & Brown, J. (2009). Shallow shelf approximation as a “sliding law” in a thermodynamically coupled ice sheet model. *Journal of Geophysical Research*, *114*, F03008. <https://doi.org/10.1029/2008JF001179>
- Bueler, E., Lingle, C. S., & Brown, J. (2007). Fast computation of a viscoelastic deformable Earth model for ice-sheet simulations. *Annals of Glaciology*, *46*(1), 97–105.
- Charbit, S., Ritz, C., & Ramstein, G. (2002). Simulations of Northern Hemisphere ice-sheet retreat: Sensitivity to physical mechanisms involved during the Last Deglaciation. *Quaternary Science Reviews*, *21*(1–3), 243–265.
- Colleoni, F., De Santis, L., Montoli, E., Olivo, E., Sorlien, C. C., Bart, P. J., et al. (2018). Past continental shelf evolution increased Antarctic ice sheet sensitivity to climatic conditions. *Scientific Reports*, *8*(1), 11,323.
- Cramer, B. S., Toggweiler, J. R., Wright, J. D., Katz, M. E., & Miller, K. G. (2009). Ocean overturning since the Late Cretaceous: Inferences from a new benthic foraminiferal isotope compilation. *Paleoceanography*, *24*, PA4216. <https://doi.org/10.1029/2008PA001683>
- de Boer, B., Dolan, A. M., Bernales, J., Gasson, E., Golledge, N. R., Sutter, J., et al. (2015). Simulating the Antarctic ice sheet in the late-Pliocene warm period: PLISMIP-ANT, an ice-sheet model intercomparison project. *The Cryosphere*, *9*, 881–903.
- de Boer, B., van de Wal, R. S. W., Bintanja, R., Lourens, L. J., & Tuenter, E. (2010). Cenozoic global ice-volume and temperature simulations with 1-D ice-sheet models forced by benthic δ¹⁸O records. *Annals of Glaciology*, *51*(55), 23–33.
- De Santis, L., Prato, S., Brancolini, G., Lovo, M., & Torelli, L. (1999). The Eastern Ross Sea continental shelf during the Cenozoic: Implications for the West Antarctic ice sheet development. *Global and Planetary Change*, *23*(1–4), 173–196.
- Depoorter, M. A., Bamber, J. L., Griggs, J. A., Lenaerts, J. T. M., Ligtenberg, S. R. M., van den Broeke, M. R., & Moholdt, G. (2013). Calving fluxes and basal melt rates of Antarctic ice shelves. *Nature*, *502*(7469), 89.
- Dolan, A. M., de Boer, B., Bernales, J., Hill, D. J., & Haywood, A. M. (2018). High climate model dependency of Pliocene Antarctic ice-sheet predictions. *Nature Communications*, *9*(1), 2799.
- Dolan, A. M., Haywood, A. M., Hill, D. J., Dowsett, H. J., Hunter, S. J., Lunt, D. J., & Pickering, S. J. (2011). Sensitivity of Pliocene ice sheets to orbital forcing. *Palaeogeography, Palaeoclimatology, Palaeoecology*, *309*(1–2), 98–110.
- Fortuin, J. P. F., & Oerlemans, J. (1990). Parameterization of the annual surface temperature and mass balance of Antarctica. *Annals of Glaciology*, *14*(1), 78–84.
- Foster, G. L., Lear, C. H., & Rae, J. W. B. (2012). The evolution of pCO₂, ice volume and climate during the middle Miocene. *Earth and Planetary Science Letters*, *341*, 243–254.
- Fretwell, P., Pritchard, H. D., Vaughan, D. G., Bamber, J. L., Barrand, N. E., Bell, R., et al. (2013). Bedmap2: Improved ice bed, surface and thickness datasets for Antarctica. *The Cryosphere*, *7*(1), 375–393.
- Gasson, E. (2013). The past relationship between temperature and sea level—From proxy records and ice sheet modeling (PhD thesis).
- Gasson, E., DeConto, R., & Pollard, D. (2015). Antarctic bedrock topography uncertainty and ice sheet stability. *Geophysical Research Letters*, *42*, 5372–5377. <https://doi.org/10.1002/2015GL064322>
- Gasson, E., DeConto, R. M., Pollard, D., & Levy, R. H. (2016). Dynamic Antarctic ice sheet during the early to mid-Miocene. *Proceedings of the National Academy of Sciences*, *113*(13), 3459–3464.

- Gasson, E., Lunt, D. J., DeConto, R., Goldner, A., Heinemann, M., Huber, M., et al. (2014). Uncertainties in the modelled CO₂ threshold for Antarctic glaciation. *Climate of the Past*, *10*(2), 451.
- Goldner, A., Herold, N., & Huber, M. (2014). The challenge of simulating the warmth of the mid-Miocene climatic optimum in CESM1. *Climate of the Past*, *10*(2), 523–536. <https://doi.org/10.5194/cp-10-523-2014>
- Greenop, R., Foster, G. L., Wilson, P. A., & Lear, C. H. (2014). Middle Miocene climate instability associated with high-amplitude CO₂ variability. *Paleoceanography*, *29*, 845–853. <https://doi.org/10.1002/2014PA002653>
- Greve, R. (2001). Glacial isostasy: Models for the response of the Earth to varying ice loads, *Continuum Mechanics and Applications in Geophysics and the Environment* (pp. 307–325). Berlin, Heidelberg: Springer.
- Herold, N., Seton, M., Müller, R. D., You, Y., & Huber, M. (2008). Middle Miocene tectonic boundary conditions for use in climate models. *Geochemistry, Geophysics, Geosystems*, *9*, Q10009. <https://doi.org/10.1029/2008GC002046>
- Hock, R. (2005). Glacier melt: A review of processes and their modelling. *Progress in Physical Geography*, *29*(3), 362–391.
- Holbourn, A., Kuhnt, W., Clemens, S., Prell, W., & Andersen, N. (2013). Middle to late Miocene stepwise climate cooling: Evidence from a high-resolution deep water isotope curve spanning 8 million years. *Paleoceanography*, *28*, 688–699. <https://doi.org/10.1002/2013PA002538>
- Huang, X., Gohl, K., & Jokat, W. (2014). Variability in Cenozoic sedimentation and paleo-water depths of the Weddell Sea basin related to pre-glacial and glacial conditions of Antarctica. *Global and Planetary Change*, *118*, 25–41.
- Huybrechts, P. (1993). Glaciological modelling of the Late Cenozoic East Antarctic ice sheet: Stability or dynamism? *Geografiska Annaler Series A Physical Geography*, *75*, 221–238.
- Huybrechts, P., Gregory, J., Janssens, I., & Wild, M. (2004). Modelling Antarctic and Greenland volume changes during the 20th and 21st centuries forced by GCM time slice integrations. *Global and Planetary Change*, *42*(1–4), 83–105.
- Jungclauss, J. H., Keenlyside, N., Botzet, M., Haak, H., Luo, J.-J., Latif, M., et al. (2006). Ocean circulation and tropical variability in the coupled model ECHAM5/MPI-OM. *Journal of Climate*, *19*(16), 3952–3972.
- Kirchner, N., Hutter, K., Jakobsson, M., & Gyllencreutz, R. (2011). Capabilities and limitations of numerical ice sheet models: A discussion for Earth-scientists and modelers. *Quaternary Science Reviews*, *30*(25–26), 3691–3704.
- Kürschner, W. M., Kvaček, Z., & Dilcher, D. L. (2008). The impact of Miocene atmospheric carbon dioxide fluctuations on climate and the evolution of terrestrial ecosystems. *Proceedings of the National Academy of Sciences*, *105*(2), 449–453.
- Langebroek, P. M., Paul, A., & Schulz, M. (2009). Antarctic ice-sheet response to atmospheric CO₂ and insolation in the Middle Miocene. *Climate of the Past*, *5*(4), 633–646.
- Langebroek, P. M., Paul, A., & Schulz, M. (2010). Simulating the sea level imprint on marine oxygen isotope records during the middle Miocene using an ice sheet–climate model. *Paleoceanography*, *25*, PA4203. <https://doi.org/10.1029/2008PA001704>
- Lear, C. H., Mawbey, E. M., & Rosenthal, Y. (2010). Cenozoic benthic foraminiferal Mg/Ca and Li/Ca records: Toward unlocking temperatures and saturation states. *Paleoceanography*, *25*, PA4215. <https://doi.org/10.1029/2009PA001880>
- Levermann, A., Albrecht, T., Winkelmann, R., Martin, M. A., Haseloff, M., & Joughin, I. (2012). Kinematic first-order calving law implies potential for abrupt ice-shelf retreat. *The Cryosphere*, *6*(2), 273.
- Levy, R. H., Meyers, S. R., Naish, T. R., Golledge, N. R., McKay, R. M., Crampton, J. S., et al. (2019). Antarctic ice-sheet sensitivity to obliquity forcing enhanced through ocean connections. *Nature Geoscience*, *12*, 132–137.
- Liebrand, D., de Bakker, A. T. M., Beddow, H. M., Wilson, P. A., Bohaty, S. M., Ruessink, G., et al. (2017). Evolution of the early Antarctic ice ages. *Proceedings of the National Academy of Sciences*, *114*, 3867–3872.
- Liebrand, D., Lourens, L. J., Hodell, D. A., de Boer, B., van de Wal, R. S. W., & Pälike, H. (2011). Antarctic ice sheet and oceanographic response to eccentricity forcing during the early Miocene. *Climate of the Past*, *7*(3), 869–880.
- Lingle, C. S., & Clark, J. A. (1985). A numerical model of interactions between a marine ice sheet and the solid earth: Application to a West Antarctic ice stream. *Journal of Geophysical Research*, *90*(C1), 1100–1114.
- Locarnini, R. A., Mishonov, A. V., Antonov, J. I., Boyer, T. P., Garcia, H. E., Baranova, O. K., et al. (2010). *World Ocean Atlas 2009, vol. 1, Temperature* (pp. 184). Washington, DC: US Gov. Printing Office.
- Lythe, M. B., & Vaughan, D. G. (2001). BEDMAP: A new ice thickness and subglacial topographic model of Antarctica. *Journal of Geophysical Research*, *106*(B6), 11,335–11,351.
- Maslin, M. A., Li, X. S., Loutre, M.-F., & Berger, A. (1998). The contribution of orbital forcing to the progressive intensification of Northern Hemisphere glaciation. *Quaternary Science Reviews*, *17*(4–5), 411–426.
- Masson-Delmotte, V., Stenni, B., Pol, K., Braconnot, P., Cattani, O., Falourd, S., et al. (2010). EPICA Dome C record of glacial and interglacial intensities. *Quaternary Science Reviews*, *29*(1–2), 113–128.
- Oerlemans, J. (1980). Continental ice sheets and the planetary radiation budget. *Quaternary Research*, *14*(3), 349–359.
- Oerlemans, J. (1984). Numerical experiments on glacial erosion. *Zeitschrift für Gletscherkunde und Glazialgeologie*, *20*, 107–126.
- Pollard, D., & DeConto, R. M. (2005). Hysteresis in Cenozoic Antarctic ice-sheet variations. *Global and Planetary Change*, *45*(1), 9–21.
- Pollard, D., DeConto, R. M., & Alley, R. B. (2015). Potential Antarctic Ice Sheet retreat driven by hydrofracturing and ice cliff failure. *Earth and Planetary Science Letters*, *412*, 112–121.
- Quiquet, A., Punge, H., Ritz, C., Fettweis, X., Kageyama, M., Krinner, G., et al. (2012). Sensitivity of a Greenland ice sheet model to atmospheric forcing fields. *The Cryosphere*, *6*, 999–1018.
- Raddatz, T. J., Reick, C. H., Knorr, W., Kattge, J., Roeckner, E., Schnur, R., et al. (2007). Will the tropical land biosphere dominate the climate–carbon cycle feedback during the twenty-first century? *Climate Dynamics*, *29*(6), 565–574.
- Reeh, N. (1991). Parameterization of melt rate and surface temperature on the Greenland ice sheet. *Polarforschung*, *59*(3), 113–128.
- Rignot, E., Jacobs, S., Mougnot, J., & Scheuchl, B. (2013). Ice-shelf melting around Antarctica. *Science*, *341*(6143), 266–270.
- Ritz, C., Rommelaere, V., & Dumas, C. (2001). Modeling the evolution of Antarctic ice sheet over the last 420,000 years: Implications for altitude changes in the Vostok region. *Journal of Geophysical Research*, *106*(D23), 31,943–31,964.
- Schodlok, M. P., Menemenlis, D., & Rignot, E. J. (2016). Ice shelf basal melt rates around Antarctica from simulations and observations. *Journal of Geophysical Research: Oceans*, *121*, 1085–1109. <https://doi.org/10.1002/2015JC011117>
- Shapiro, N. M., & Ritzwoller, M. H. (2004). Inferring surface heat flux distributions guided by a global seismic model: Particular application to Antarctica. *Earth and Planetary Science Letters*, *223*(1), 213–224.
- Shevenell, A. E., Kennett, J. P., & Lea, D. W. (2008). Middle miocene ice sheet dynamics, deep-sea temperatures, and carbon cycling: A Southern Ocean perspective. *Geochemistry, Geophysics, Geosystems*, *9*, Q02006. <https://doi.org/10.1029/2007GC001736>
- Siegert, M. J. (2008). Antarctic subglacial topography and ice-sheet evolution. *Earth Surface Processes and Landforms*, *33*(4), 646–660.
- Stap, L. B., van de Wal, R. S. W., de Boer, B., Bintanja, R., & Lourens, L. J. (2016). The MMCO-EOT conundrum: Same benthic $\delta^{18}\text{O}$, different CO₂. *Paleoceanography*, *31*, 1270–1282. <https://doi.org/10.1002/2016PA002958>

- Stap, L. B., van de Wal, R. S. W., de Boer, B., Bintanja, R., & Lourens, L. J. (2017). The influence of ice sheets on temperature during the past 38 million years inferred from a one-dimensional ice sheet–climate model. *Climate of the Past*, *13*(9), 1243.
- Stärz, M. (2013). Past Earth System Sensitivity: Forcing and feedback mechanisms on orbital timescales using regional and global models (PhD thesis), Universität Bremen, Bremen, Germany.
- Stärz, M., Jokat, W., Knorr, G., & Lohmann, G. (2017). Threshold in North Atlantic-Arctic Ocean circulation controlled by the subsidence of the Greenland-Scotland Ridge. *Nature Communications*, *8*, 15681.
- Stocchi, P., Escutia, C., Houben, A. J. P., Vermeersen, B. L. A., Bijl, P. K., Brinkhuis, H., et al. (2013). Relative sea-level rise around East Antarctica during Oligocene glaciation. *Nature Geoscience*, *6*(5), 380–384.
- Sutter, J., Gierz, P., Grosfeld, K., Thoma, M., & Lohmann, G. (2016). Ocean temperature thresholds for Last Interglacial West Antarctic Ice Sheet collapse. *Geophysical Research Letters*, *43*, 2675–2682. <https://doi.org/10.1002/2016GL067818>
- Uppala, S. M., Källberg, P. W., Simmons, A. J., Andrae, U., Bechtold, V., Fiorino, M., et al. (2005). The ERA-40 re-analysis. *Quarterly Journal of the Royal Meteorological Society*, *131*(612), 2961–3012.
- van de Berg, W. J., van den Broeke, M., Ettema, J., van Meijgaard, E., & Kaspar, F. (2011). Significant contribution of insolation to Eemian melting of the Greenland ice sheet. *Nature Geoscience*, *4*(10), 679–683.
- Wilson, D. S., Jamieson, S. S. R., Barrett, P. J., Leitchkov, G., Gohl, K., & Larter, R. D. (2012). Antarctic topography at the Eocene–Oligocene boundary. *Palaeogeography, Palaeoclimatology, Palaeoecology*, *335*, 24–34.
- Wilson, D. S., Pollard, D., DeConto, R. M., Jamieson, S. S. R., & Luyendyk, B. P. (2013). Initiation of the West Antarctic Ice Sheet and estimates of total Antarctic ice volume in the earliest Oligocene. *Geophysical Research Letters*, *40*, 4305–4309. <https://doi.org/10.1002/grl.50797>
- Winkelmann, R., Martin, M. A., Haseloff, M., Albrecht, T., Bueller, E., Khroulev, C., & Levermann, A. (2011). The Potsdam Parallel Ice Sheet Model (PISM-PIK) Part 1: Model description. *The Cryosphere*, *5*, 715–726.
- Yamagishi, T., Abe-Ouchi, A., Saito, F., Segawa, T., & Nishimura, T. (2005). Re-evaluation of paleo-accumulation parameterization over Northern Hemisphere ice sheets during the ice age examined with a high-resolution AGCM and a 3-D ice-sheet model. *Annals of Glaciology*, *42*, 433–440.
- Yan, Q., Zhang, Z., & Wang, H. (2016). Investigating uncertainty in the simulation of the Antarctic ice sheet during the mid-Piacenzian. *Journal of Geophysical Research: Atmospheres*, *121*, 1559–1574. <https://doi.org/10.1002/2015JD023900>
- Zachos, J. C., Dickens, G. R., & Zeebe, R. E. (2008). An early Cenozoic perspective on greenhouse warming and carbon-cycle dynamics. *Nature*, *451*(7176), 279–283.
- Zachos, J. C., Shackleton, N. J., Revenaugh, J. S., Pälike, H., & Flower, B. P. (2001). Climate response to orbital forcing across the Oligocene-Miocene boundary. *Science*, *292*(5515), 274–278.
- Zhang, Y. G., Pagani, M., Liu, Z., Bohaty, S. M., & DeConto, R. (2013). A 40-million-year history of atmospheric CO₂. *Philosophical Transactions of the Royal Society A*, *371*(2001), 20130096.